Electronic Structure in the Intervalence Transfer Absorption Band of a Mixed-Valence Dimer

Edward M. Kober, Kenneth A. Goldsby, D. N. S. Narayana, and Thomas J. Meyer*

Contribution from the Department of Chemistry, The University of North Carolina, Chapel Hill, North Carolina 27514. *Received July 2, 1982*

Abstract: Electronic structure has been observed in the intervalence transfer (IT) absorption band of the weakly coupled mixed-valence dimer $[(bpy)_2ClOs^{II}(PPh_2CH_2Ph_2P)Os^{III}Cl(bpy)_2]^{3+}$ (bpy is 2,2′-bipyridine). The origin of the structure lies in the large spin–orbit (SO) coupling constant (λ_{Os}) for osmium which leads to well separated SO states for the Os^{III} $d\pi^5$ electronic configuration. For Os^{III}–bpy monomers, low-energy $d\pi \rightarrow d\pi$ transitions between the SO states are observed in the near-infrared (near-IR). Optical electron transfer in the mixed-valence dimer results in the formation of a "new" Os(III) site in one of three possible SO states (1E′, 2E′, or 3E′), and hence the IT manifold should contain three components separated by the energy differences between the SO states at the Os(III) site. In addition to the expected $d\pi$–$d\pi$ absorption bands, the spectrum of the Os(II)–Os(III) dimer in the near-IR shows two broad, solvent-dependent bands which are assignable to IT transitions. The bands are separated in energy by approximately the energy difference between the two lowest SO states as expected. Calculations on the expected position of the third component indicate that it should occur in a spectral region obscured by intense metal-to-ligand charge-transfer bands. By analogy, it is argued that the single IT band observed for the Ru dimer $[(bpy)_2ClRu^{II}(PPh_2CH_2Ph_2P)Ru^{III}Cl(bpy)_2]^{3+}$ also consists of a manifold of three closely spaced components but that they are not resolvable at room temperature because of the smaller SO coupling constant for Ru ($\lambda_{Ru} \approx {}^1/_3\lambda_{Os}$). For the Ru dimer, the IT band intensity is expected to be dominated by the transition $Ru^{II}(A_1)$–$Ru^{III}(1E') \rightarrow Ru^{III}(2E')$–$Ru^{II}(A_1)$, which occurs at ca. 1700 cm^{-1} above the lowest energy transition $Ru^{II}(A_1)$–$Ru^{III}(1E') \rightarrow Ru^{III}(1E')$–$Ru^{II}(A_1)$. As a consequence, the use of the IT band energy to estimate the classical inner-sphere vibrational trapping energy $\chi_i/4$ from solvent dependence studies is an overestimate for this and related dimers.

Broad, solvent-dependent, low-energy absorption bands are frequently observed in ligand-bridged, mixed-valence dimers, e.g., $(NH_3)_5Ru^{II}(4,4'\text{-bpy})Ru^{III}(NH_3)_5^{5+}$ and $(bpy)_2ClRu^{II}(pyr)$-$Ru^{III}Cl(bpy)_2^{3+}$ (4,4′-bpy is 4,4′-bipyridine, bpy is 2,2′-bipyridine and pyr is pyrazine). The bands, which are assignable to optically induced electron transfer between the different oxidation state sites (eq 1), have been termed intervalence transfer (IT) or metal–metal charge-transfer (MMCT) bands.[1-4] In the limit of

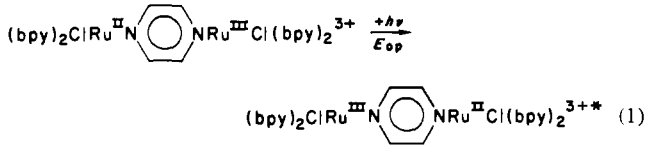

(1)

weak electronic coupling, where thermal electron transfer between sites is slow on the vibrational time scale, Hush has given classical equations for the band width and solvent dependences of MMCT bands. The equations have proven to be of value in accounting for experimental bandwidths, in accounting for the variations of absorption band energies with solvent,[1-5] and for relating the properties of the bands to analogous thermal electron transfer processes.[6]

We have been working with ground- and excited-state complexes of osmium(II) and ground-state complexes of osmium(III) in which spin–orbit (SO) coupling plays an important role in determining electronic structure and hence spectral properties.[7] In symmetries lower than O_h, the combination of the lowered symmetry and SO coupling leads to a splitting of the $d\pi$ core into a set of three d orbitals, largely $d\pi$ in character. For a low-spin, d^5 system such as Ru(III) or Os(III), the net effect is to create three orbitally nondegenerate SO states within the d^5 core: a ground state (1E′) and two excited states (2E′, 3E′) whose relative energy spacings depend on the magnitude of the SO coupling constant and the properties of the surrounding ligands.[8] As a consequence of the splitting of the $d\pi$ core, intervalence transfer in a mixed-valence dimer having the configuration M^{II}-$(d\pi^6)$–$M^{III}(d\pi^5)$ can result in the formation of a "new" M(III) site in any one of the three SO states. If the spacing between SO states is sufficiently large, their presence should be manifested in the appearance of structure in the IT absorption spectrum.

A number of groups, including our own, have reported the appearance of IT bands in Ru^{II}–Ru^{III} mixed-valence dimers. In these spectra, the IT bands appear as a single, featureless absorption band;[1-3,5,9,10] note Figure 1, where the IT band is shown for the dimer $[(bpy)_2ClRu^{II}(PPh_2CH_2Ph_2P)Ru^{III}Cl(bpy)_2]^{3+}$.[10] In retrospect, the lack of structure for the Ru dimers is a consequence of the fact that the individual components are close in energy and not resolvable at room temperature. In order to observe electronic structure, we have turned to a mixed-valence dimer of Os, $[(bpy)_2ClOs^{II}(PPh_2CH_2Ph_2P)Os^{III}Cl(bpy)_2]^{3+}$. The choice of Os was dictated by its larger SO coupling constant ($\lambda_{Os} \approx 3200$ cm^{-1}; $\lambda_{Ru} \approx 1200$ cm^{-1}).[11] In particular, the phosphine-bridged dimer was appealing because of the expected weak electronic coupling through the saturated bridging ligand and because of the absence of low-energy $Os^{II} \rightarrow$ bridging ligand transitions which could obscure the spectral region of interest.

Multiple transitions have been observed in the IT band spectral region for mixed-valence dimers of both Ru[12] and Os.[13] However, in these dimers there is evidence for strong electronic coupling

(1) (a) Meyer, T. J. In "Mixed-Valence Compounds"; Brown, D. M., Ed.; D. Reidel Publishing Co.: Dordrecht, Holland, 1980, pp 75–113. (b) Meyer, T. J. *Prog. Inorg. Chem.* **1983**, *30*, 389.
(2) Taube, H. *Ann. N. Y. Acad. Sci.* **1978**, *313*, 481.
(3) Meyer, T. J. *Ann. N. Y. Acad. Sci.* **1978**, *313*, 496.
(4) (a) Hush, N. S. *Prog. Inorg. Chem.* **1967**, *8*, 391. (b) Hush, N. S. *Electrochim. Acta* **1968**, *13*, 1005. (c) Hush, N. S. *Chem. Phys.* **1975**, *10*, 361.
(5) (a) Powers, M. J.; Meyer, T. J. *J. Am. Chem. Soc.* **1980**, *102*, 1289. (b) Sullivan, B. P.; Curtis, J. C.; Kober, E. M.; Meyer, T. J. *Nouv. J. Chim.* **1980**, *4*, 643. (c) Meyer, T. J. *Acc. Chem. Res.* **1978**, *11*, 94.
(6) (a) Curtis, J. C.; Sullivan, B. P.; Meyer, T. J. *Inorg. Chem.* **1980**, *19*, 3833. (b) Curtis, J. C.; Meyer, T. J. *Ibid.* **1982**, *21*, 1562. (c) Meyer, T. J. *Chem. Phys. Lett.* **1979**, *64*, 417.
(7) (a) Kober, E. M.; Sullivan, B. P.; Caspar, J. V.; Meyer, T. J., manuscript in preparation. (b) Kober, E. M.; Meyer, T. J. *Inorg. Chem.* **1982**, *21*, 3967.
(8) Each of the SO states is a Kramer's doublet and hence transforms as $E_{1/2}$ in the C_1' double group.
(9) For example: (a) Gulka, R.; Isied, S. S. *Inorg. Chem.* **1980**, *19*, 2842. (b) Sedney, D.; Ludi, S. *Inorg. Chim. Acta* **1981**, *47*, 153. (c) Stein, C. A.; Taube, H. *J. Am. Chem. Soc.* **1981**, *103*, 643. (d) Stein, C. A.; Lewis, N. A.; Seitz, G. *Ibid.* 1982, *104*, 2596. (e) Heath, G. A.; Lindsay, A. J.; Stephenson, T. A.; Vattis, D. K. *J. Organomet. Chem.* **1982**, *233*, 353.
(10) Sullivan, B. P.; Meyer, T. J. *Inorg. Chem.* **1980**, *19*, 752.
(11) Goodman, B. A.; Raynor, J. B. *Adv. Inorg. Radiochem.* **1970**, *13*, 192.
(12) Juss, S.; Reust, H.; Ludi, A. *J. Am. Chem. Soc.* **1981**, *103*, 981.
(13) (a) Magnuson, R. H.; Taube, H. *J. Am. Chem. Soc.* **1972**, *94*, 7213. (b) Richardson, D. E.; Sen, J. P.; Buhr, J. D.; Taube, H. *Inorg. Chem.* **1982**, *21*, 3136.

0002-7863/83/1505-4303$01.50/0

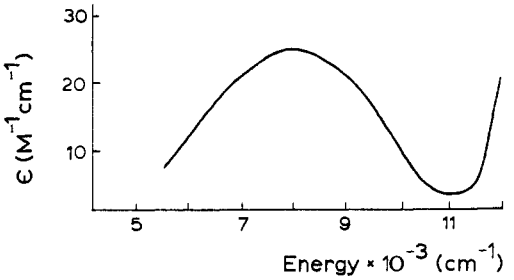

Figure 1. Near-IR absorption spectra for $[(bpy)_2ClRu^{II}(PPh_2CH_2Ph_2P)Ru^{III}Cl(bpy)_2]^{3+}$. Redrawn from ref 10.

between sites and a detailed interpretation of the spectra has not been given. An advantage of the dimeric osmium system studied here is that since the electronic coupling between sites is relatively weak, it is possible to develop a detailed model to explain the low-energy electronic transitions.

Experimental Section

Measurements. Ultraviolet, visible, and near-infrared spectra were recorded by using either a Cary Model 14 or a Varian Series 634 spectrophotometer. Electrochemical measurements were made vs. the saturated sodium chloride calomel electrode (SSCE) at 25 ± 2 °C and are uncorrected for junction potential effects. The $E_{1/2}$ values for reversible couples were calculated from half the sum of the E_p values for the anodic and cathodic waves from cyclic voltammetry. The measurements were made by using a PAR Model 173 potentiostat for potential control with a PAR Model 175 universal programmer as a sweep generator for voltammetry measurements. Values for n, where n is the total number of electrons transferred per Os ion site in exhaustive oxidative electrolyses at constant potential, were calculated after the total area under current vs. time curves for the complete reaction was measured. The reactions were considered complete after the current had fallen to 1% of the initial value. Values of n for the reduction of the oxidized product were calculated on the basis of the same criterion. All cyclic voltammetry measurements were performed at glassy carbon disk electrodes, and all coulometry measurements were performed at platinum screen electrodes. Burdick & Jackson acetonitrile was employed as the electrochemical solvent and 0.1 M tetraethylammonium perchlorate (TEAP) as the electrolyte. Elemental analyses were performed by Integral Microlabs, Raleigh, NC.

Materials. TEAP, $[N(C_2H_5)_4](ClO_4)$, was prepared as described previously,[14] recrystallized from hot ethanol/water four times, and vacuum dried at 70 °C for 10 h. Burdick & Jackson acetonitrile was used for electrochemical measurements without drying or special treatment, except to reseal the bottle with Parafilm after each use and store in a dark place. Deuterated acetonitrile was purchased from Aldrich. All solvents used for preparations were reagent grade and used without further purification. Dppm, $PPh_2CH_2Ph_2P$, was purchased from Strem Chemical Co. and used as received.

Preparations. ***cis*-(bpy)$_2$OsCl$_2$.** Although the original procedure of Dwyer et al.[15] gives reasonable yields, we have developed a modified procedure using ethylene glycol as solvent which gives better yields.[16]

$[(bpy)_2ClOs(PPh_2CH_2Ph_2P)OsCl(bpy)_2](PF_6)_2$. To 30 mL of 1:1 EtOH/water were added *cis*-$(bpy)_2OsCl_2$ (0.106 g, 0.185 mmol) and $PPh_2CH_2Ph_2P$ (0.036 g, 0.094 mmol). The mixture was heated at reflux under Ar for 24 h while magnetic stirring was maintained. After this time the mixture was allowed to cool, and a solution of NH_4PF_6 (0.3 g, 1.8 mmol) dissolved in 30 mL of water was filtered into the mixture. The mixture was stirred an additional 20 min. The total volume of solution was then reduced to approximately one-third on a rotary evaporator. The resulting dark green precipitate was isolated by suction filtration, washed well with water, toluene, and diethyl ether, and then air-dried. The crude reaction product was chromatographed on a 4 cm × 13 cm column of alumina packed in 1:1 $CH_3CN/C_6H_5CH_3$. The dark green solid was dissolved in a minimum amount of 1:1 $CH_3CN/C_6H_5CH_3$ (~3 mL) and loaded onto the column with a pipet. Elution with 1:1 $CH_3CN/C_6H_5CH_3$ gave a dark green band of the dimer which was preceded by two light green bands and followed by a bright orange luminescent band.

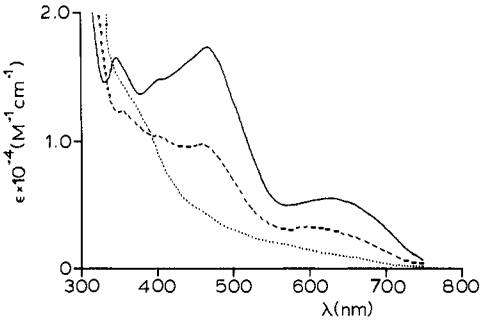

Figure 2. Electronic spectra of $[(bpy)_2ClOs(PPh_2CH_2Ph_2P)OsCl(bpy)_2]^{2+}$ (—), $[(bpy)_2ClOs(PPh_2CH_2Ph_2P)OsCl(bpy)_2]^{3+}$ (---), and $[(bpy)_2ClOs(PPh_2CH_2Ph_2P)OsCl(bpy)_2]^{4+}$ (···) in acetonitrile.

An aqua blue band remained at the top of the column. The dark green band was collected and taken to dryness on a rotary evaporator. The complex was redissolved in a minimum amount of CH_3CN and precipitated with Et_2O to yield a dark green powdery solid in 25% yield. Anal. Calcd for $[(bpy)_2ClOs(PPh_2CH_2Ph_2P)OsCl(bpy)_2](PF_6)_2 \cdot H_2O$: C, 44.04; H, 3.19; N, 6.32. Found: C, 44.02; H, 3.21; N, 6.33.

$[(bpy)_2ClOs(PPh_2CH_2Ph_2P)OsCl(bpy)_2](PF_6)_4$. $[(bpy)_2ClOs(PPh_2CH_2Ph_2P)OsCl(bpy)_2](PF_6)_2$ (0.050 g, 0.028 mmol) was dissolved in 35 mL of 2:1 CH_3CN/water and ~5 mL of a saturated aqueous NH_4PF_6 solution was added while magnetic stirring was maintained. The mixture was filtered, and ~1 mL of Br_2 was added to the stirring solution. Immediately upon addition of Br_2, the solution turned from dark green to brown. Ar was bubbled through the stirring mixture for ~45 min in order to remove excess Br_2. At the end of this period 20 mL of water was added to the mixture and the solution volume was reduced to ca. 30 mL on a rotary evaporator. The brown precipitate was isolated by suction filtration, washed well with water and Et_2O, and then air-dried. A nearly quantitative yield of the [III,III] dimer was obtained.

$[(bpy)_2ClOs(PPh_2CH_2Ph_2P)OsCl(bpy)_2](PF_6)_3$. $[(bpy)_2ClOs(PPh_2CH_2Ph_2P)OsCl(bpy)_2](PF_6)_2$ (0.024 g, 0.014 mmol) and $[(bpy)_2ClOs(PPh_2CH_2Ph_2P)OsCl(bpy)_2](PF_6)_4$ (0.028 g, 0.014 mmol) were dissolved in 20 mL of CH_3CN, and magnetic stirring was maintained for ~15 min. The mixture was then added dropwise to ~400 mL of rapidly stirring Et_2O, precipitating the mixed-valence dimer. The dull green powdery solid was isolated by suction filtration in 70% yield and air-dried for several minutes.

Results

Cyclic voltammetry of the Os(II)–Os(II) dimer in CH_3CN with 0.1 M $[N(C_2H_5)_4](ClO_4)$ as supporting electrolyte and a scan rate of 200 mV/s showed two reversible anodic waves at $E_{1/2,1} = 0.54$ V ($\Delta E_p = 65$ mV) and $E_{1/2,2} = 0.67$ V ($\Delta E_p = 60$ mV).[17] Oxidative coulometry at 0.9 V and rereduction at 0.0 V both yielded n values of 2 within experimental error without decomposition of the dimer. From the separation between the redox couples of $\Delta E_{1/2} = 0.13$ V, $K_{com} = 160$ can be calculated for the comproportionation equilibrium in eq 2. It should be noted that this

$$[(bpy)_2ClOs(PPh_2CH_2Ph_2P)OsCl(bpy)_2]^{2+} + [(bpy)_2ClOs(PPh_2CH_2Ph_2P)OsCl(bpy)_2]^{4+} \rightleftharpoons 2[(bpy)_2ClOs(PPh_2CH_2Ph_2P)OsCl(bpy)_2]^{3+} \quad (2)$$

is very close to the value of $\Delta E_{1/2}$ observed for the analogous Ru dimer (0.14 V);[9] however, the couples for the Os dimer are at approximately 400 mV lower potential, which is commonly observed in comparing analogous Os and Ru couples.[7a,18] It is the lower potentials for the Os system that allow the [3,3] dimer to be generated by Br_2 oxidation, as in eq 3.

$$[(bpy)_2ClOs(PPh_2CH_2Ph_2P)OsCl(bpy)_2]^{2+} + Br_2 \rightarrow [(bpy)_2ClOs(PPh_2CH_2Ph_2P)OsCl(bpy)_2]^{4+} + 2Br^- \quad (3)$$

The UV–vis spectra of the [2,2], [2,3], and [3,3] ions in acetonitrile solution are shown in Figure 2. As is commonly observed with mixed-valence ions, the spectrum of the [2,3] ion is comprised

(14) Sawyers, D. T.; Roberts, J. L. "Experimental Electrochemistry for Chemists"; Wiley: New York, 1974.
(15) Buckingham, D. A.; Dwyer, F. P.; Goodwin, H. A.; Sargeson, A. M. *Aust. J. Chem.* **1964**, *17*, 325.
(16) Kober, E. M.; Sullivan, B. P.; Caspar, J. V.; Meyer, T. J., manuscript in preparation.
(17) $E_{1/2} = (E_{p,a} - E_{p,c})/2$ where potentials were measured vs. the saturated sodium chloride electrode. The ΔE_p values, $\Delta E_p = E_{p,a} - E_{p,c} = 60 - 65$ mV, are characteristic of reversible one-electron processes under the experimental conditions used.
(18) Taube, H. *Pure Appl. Chem.* **1979**, *51*, 901.

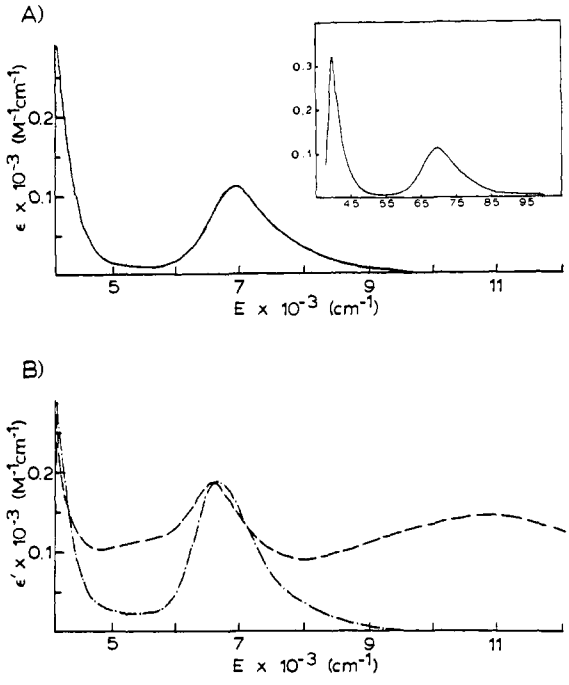

Figure 3. Near-IR absorption spectra for $[(bpy)_2ClOs(PPh_3)]^{2+}$ (A), and $[(bpy)_2ClOs(PPh_2CH_2Ph_2P)OsCl(bpy)_2]^{n+}$ (B, (---) $n = 3$, (-·-) $n = 4$). In A, insert has been inclued to show more completely both SO bands. In B, $\epsilon' = \epsilon$ per Os(III) site.

Table I. Near-Infrared Spectral Data for the $d\pi \rightarrow d\pi$ Transitions in CD_3CN

complex	$10^{-3}\lambda_{max}$, cm^{-1} (ϵ_{max}, M^{-1} cm^{-1})	
	$1E' \rightarrow 2E'$	$1E' \rightarrow 3E'$
$[(bpy)_2ClOs(PPh_3)]^{2+}$	3.98 (320)	6.99 (110)
$[(bpy)_2ClOs)_2PPh_2CH_2Ph_2P]^{3+}$	3.98 (420)	6.50 (190)
$[(bpy)_2ClOs)_2PPh_2CH_2Ph_2P]^{4+}$	3.98 (640)	6.65 (380)

of bands present in both the [2,2] and [3,3] ions, with no new spectral features. Near-infrared (near-IR) spectra for the [2,3] and [3,3] forms of the dimer, as well as for the related monomer $[(bpy)_2ClOs(PPh_3)]^{2+}$, were obtained in acetonitrile-d_3 (see Figure 3), and near-IR spectra of the [2,3] dimer were recorded in several other nondeuterated solvents. As is apparent from Figure 3, the near-IR spectra for these ions is considerably more complex than spectra encountered for the analogous Ru dimers which immediately suggests a complexity in electronic structure.

Discussion

Assignment of the Low-Energy Spectrum. The low-energy bands observed in the near-IR spectrum of monomeric Os(III) complexes have been assigned to $d\pi \rightarrow d\pi$ transitions between the three SO states of the d^5 core.[19,20] The bands in the spectrum of $[(bpy)_2ClOs(PPh_3)]^{2+}$ at 6990 and 3980 cm^{-1} correspond to the $1E' \rightarrow 3E'$ and $1E' \rightarrow 2E'$ transitions, respectively (see Table I). Note that these same transitions occur for the [3,3] and [2,3] forms of the dimer $[(bpy)_2ClOs(PPh_2CH_2Ph_2P)OsCl(bpy)_2]^{2+}$ at roughly the same energies. However, the near-IR spectrum of the [2,3] dimer shows additional absorption features: (1) a clearly resolved band at 10800 cm^{-1} and (2) a region of broad absorption between the two $d\pi$–$d\pi$ bands.

In order to resolve the region of broad absorption in the near-IR spectrum of the [2,3] dimer, a difference spectrum was obtained by subtracting out the $d\pi$–$d\pi$ bands. The most direct approach is to subtract half of the intensity of the [3,3] spectrum from the [2,3] spectrum,[21] and the result of this procedure is shown in

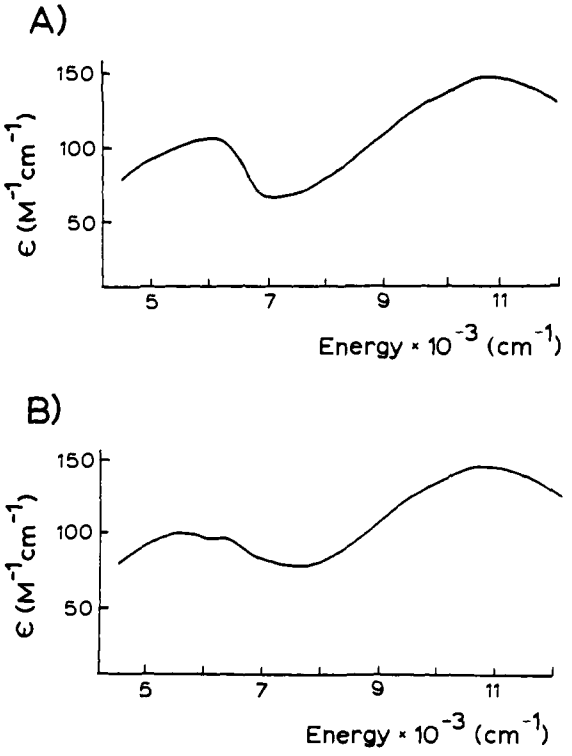

Figure 4. Spectrum of $[(bpy)_2ClOs(PPh_2CH_2Ph_2P)OsCl(bpy)_2]^{3+}$ after subtraction of the $d\pi$–$d\pi$ bands. (A) Result of direct subtraction of one-half of the [3,3] spectrum from the [2,3] spectrum. (B) Result of shifting the 6650 cm^{-1} band in the [3,3] spectrum 150 cm^{-1} to lower energy and then subtracting half of the [3,3] spectrum from the [2,3] spectrum.

Figure 4A. The presence of a second band is clearly revealed, though it is somewhat misshapen. A problem with the simple substraction procedure is that the $d\pi$–$d\pi$ bands do not occur at the same energy in the two dimers. For the [3,3] dimer the higher energy band is 150 cm^{-1} higher in energy than the band for the [2,3] dimer. Shifting this band 150 cm^{-1} to lower energy and then subtracting the two spectra gives the result shown in Figure 4B. The resulting spectrum is much smoother than the first, and the bands appear more nearly Gaussian in shape, as they should be. The shift in $d\pi$–$d\pi$ band energy between dimers is not unexpected since in one case the Os(III) site is bridged to an Os(III) and in the other it is bridged to an Os(II). The higher charge and weaker $d\pi$ donation of Os(III) relative to Os(II) should increase the π acidity of the bridging dppm ligand, causing the $d\pi$–$d\pi$ bands to move to slightly higher energy in the [3,3] dimer.[19,20]

The resulting difference spectrum shows two broad bands which, as described below, are assignable to different electronic components of the IT transition shown in eq 4. For the band at 10800

$$[(bpy)_2ClOs^{II}(PPh_2CH_2Ph_2P)Os^{III}Cl(bpy)_2]^{3+} \xrightarrow{h\nu} [(bpy)_2ClOs^{III}(PPh_2CH_2Ph_2P)Os^{II}Cl(bpy)_2]^{3+*} \quad (4)$$

cm^{-1}, which is clearly distinct in the original spectrum, the theoretical value of $\Delta\nu_{1/2}$ (the bandwidth at half-height) calculated by using eq 5[4] is 4.0×10^3 cm^{-1}. In the bandwidth calculation a value of $\Delta E = 4000$ cm^{-1} was used since, as discussed below, the band is assignable to an IT transition which gives the Os(III) site in the excited 2E′ SO state.

$$\Delta\nu_{1/2} = (2.31 \times 10^3(E_{op} - \Delta E))^{1/2} \text{ (in } cm^{-1}) \quad (5)$$

(19) Kober, E. M.; Meyer, T. J., manuscript in preparation.
(20) Kober, E. M. Ph.D. Thesis, University of North Carolina, 1982.

(21) The difference spectrum was obtained in the following way. A spectrum of a sample of the [3,3] dimer was obtained and then an excess of the [2,2] dimer was added. Neglecting that the comproportionation is not complete, the resulting solution should have a concentration of [2,3] dimer that is twice that of the original [3,3] concentration plus an undetermined concentration of [2,2] dimer which does not absorb in the spectral region of interest. The difference spectrum was obtained by subtracting the two spectra.

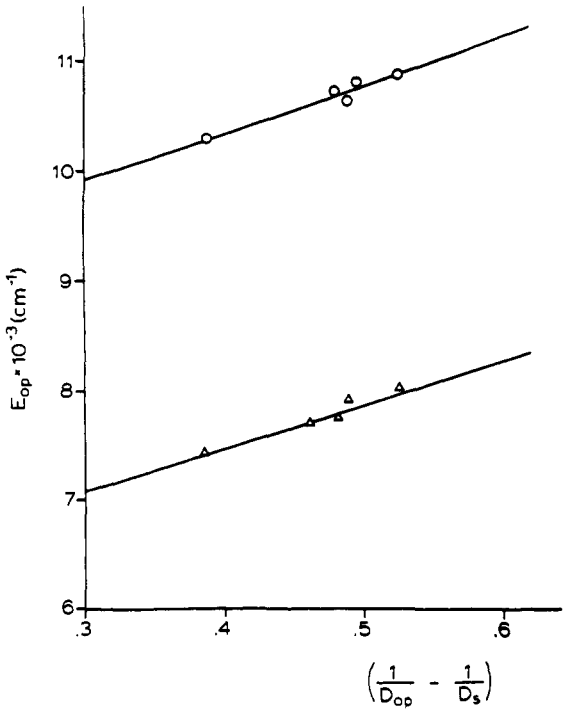

Figure 5. Plot of $(1/D_{op} - 1/D_s)$ vs. E_{op} for the higher energy IT band for $[(bpy)_2ClOs(PPh_2CH_2Ph_2P)OsCl(bpy)_2]^{3+}$ (O) and vs. λ_{max} of the MMCT absorption manifold for $[(bpy)_2ClRu(PPh_2CH_2Ph_2P)RuCl(bpy)_2]^{3+}$ (Δ).[8]

Equation 5 was derived for a harmonic oscillator in the classical limit. The calculated value is less than the experimental value of 6.0×10^3 cm^{-1} obtained by doubling the half-bandwidth of the low-energy side of the band. The experimental bandwidth is expected to be somewhat increased due to the presence of the second band at ca. 6000 cm^{-1} and the assumptions involved in deriving eq 5.[4a]

As can be seen from the data in Figure 5, the band energy of the higher energy band varies linearly with $(1/D_{op} - 1/D_s)$ where D_{op} and D_s are the optical and static dielectric constants of the medium (the dπ–dπ bands are at best slightly solvent dependent). Linear variations of optical band energy E_{op} with $(1/D_{op} - 1/D_s)$ have been observed for related Ru dimers, including the analogue of the Os dimer, $[(bpy)_2ClRu^{II}(PPh_2CH_2Ph_2P)Ru^{III}Cl(bpy)_2]^{3+}$,[10] as shown in Figure 5 for purposes of comparison.

The basis for the predicted variation of E_{op} with $(1/D_{op} - 1/D_s)$ comes from the application of dielectric continuum theory[4,5] to the effect of solvent polarization on E_{op}. The result is shown in eq 6 as χ_0, which is four times the classical vibrational trapping

$$\chi_0 = \tfrac{1}{2}(1/D_{op} - 1/D_s)\int (\vec{D}_f - \vec{D}_i)^2\, dV \qquad (6)$$

energy of the solvent. $\vec{D}_i$ and $\vec{D}_f$ are the electric displacement vectors characteristic of the charge distributions in the absence of a medium before and after electron transfer occurs, and the integration is over the volume surrounding the ions. In defining the electric field vectors in eq 6, the integral contains information about the structure of the dimer; integration of eq 6 for the case of nonpenetrating spheres of radidi a_1 and a_2 and internuclear separation d gives eq 7[4,22] which simplifies to eq 7a for a case like

$$\chi_0 = e^2\left(\frac{1}{2a_1} + \frac{1}{2a_2} + \frac{1}{d}\right)(1/D_{op} - 1/D_s) \qquad (7)$$

$$\chi_0 = e^2\left(\frac{1}{a_1} - \frac{1}{d}\right)(1/D_{op} - 1/D_s) \qquad (7a)$$

the Os dimer where $a_1 \approx a_2$. In the context of assigning the low-energy band in the Os dimer spectrum as an IT band, it is important to note that the plot of $(1/D_{op} - 1/D_s)$ vs. E_{op} for the analogous Ru dimer has the same slope within experimental error (see Figure 5) as would have been predicted from eq 7, since the Ru and Os dimers are expected to have virtually identical structures (see below). Unfortunately, the lower energy band for the Os dimer is not sufficiently resolved for meaningful bandwidth or solvent dependence results to be obtained.

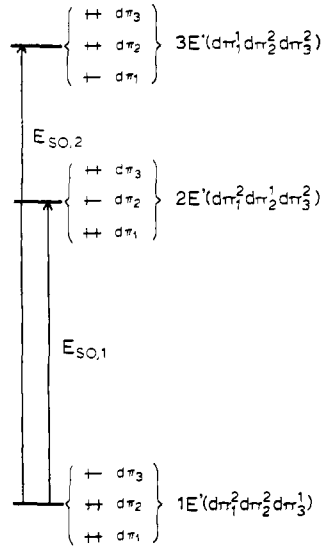

Figure 6. Schematic energy level diagram showing the energy relationships for the dπ → dπ transitions between the Os(III) SO states 1E′, 2E′, and 3E′.

The assignment of the low-energy bands in the difference spectrum as different components of an IT manifold can also be justified on the basis of energy arguments. Optical electron transfer from the initial Os(II) site to the initial Os(III) results in the formation of the new Os(III) site in one of three possible SO states, 1E′, 2E′, or 3E′ (note Figure 6), resulting in multiple components in the IT band region. Application of the Franck–Condon principle shows that for all three transitions, optical excitation leads to charge-transfer products in nonequilibrium vibrational environments—Os(II) in the coordination environment for Os(III) and vice versa. Neglecting the effects of electronic delocalization, which will be discussed below, the relationship between the energy of the optical transition and the vibrational energy is $E_{op} = \chi$ where $\chi/4$ is the classical vibrational trapping energy. As noted above, χ includes contributions from both intramolecular (χ_i) and solvent (χ_0) vibrations. In the classical dielectric continuum limit, χ_0 is given by eq 6. χ_i is given by eq 8,[23] where the summation is over all intramolecular vibrations and

$$\chi_i = \frac{1}{2}\sum_j k_j(\Delta Q_j)^2 = \frac{1}{2}\sum_j \hbar\omega_j\Delta_j^2 \qquad (8)$$

k_j is the force constant for vibration j, ΔQ_j is the difference in equilibrium displacement coordinate for vibration j between Os(II) and Os(III), $\hbar\omega_j = h\nu_j$ is the quantum spacing between vibrational levels, $\Delta_j = (\Delta Q_j)(M_j\omega_j/\hbar)^{1/2}$ is the dimensionless fractional coordinate difference at equilibrium between Os(II) and Os(III), and M_j is the reduced mass for vibration j. It is apparent from eq 8 that the only vibrations that contribute to χ_i are the so-called "trapping vibrations" for which Δ^2, $(\Delta Q)^2 \neq 0$. For the two higher energy optical transitions, the optical energy includes the energy of the excited SO states above the ground SO state in addition to χ. The various energy relationships are illustrated in Figure 7 for the three transitions. Figure 7 is drawn assuming the same values of χ are appropriate for all three transitions.

While χ_0 is expected to be roughly the same for all three IT transitions, the values for χ_i could, in fact, be very different. In

(22) Marcus, R. A. *Annu. Rev. Phys. Chem.* **1964**, *15*, 155.

(23) (a) Kestner, N. R.; Logan, J.; Jortner, J. *J. Phys. Chem.* **1974**, *78*, 2148. (b) Englman, R.; Jortner, J. *J. Mol. Phys.* **1970**, *18*, 145.

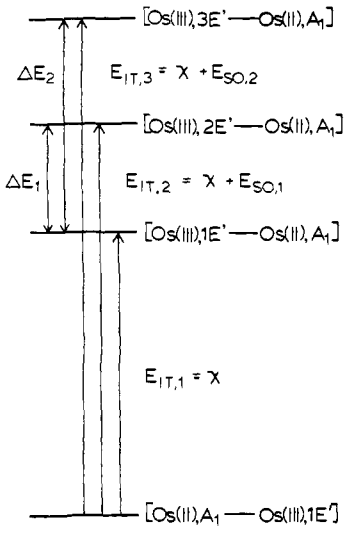

Figure 7. Energy diagram depicting the three MMCT transitions for $[(bpy)_2ClOs(PPh_2CH_2Ph_2P)OsCl(bpy)_2]^{3+}$. Note that $\Delta E_1 = E_{SO,1}$ and $\Delta E_2 = E_{SO,2}$ from Figure 6.

particular, the bandwidth for the Os(III)-based transition, $1E' \rightarrow 2E'$, is relatively narrow (Figure 3A), showing that significant distortions do not exist between the thermally equilibrated structures of the $1E'$ and $2E'$ SO states. Because the SO transitions are metal localized, negligible contributions to their bandwidth are expected from solvent. As a consequence of the narrow bandwidth for the $1E' \rightarrow 2E'$ transition, χ_i values for the first two IT transitions should be similar. However, the bandwidth for the transition $1E' \rightarrow 3E'$ is noticeably broader (Figure 3A), showing that significant differences exist between the equilibrium geometries of the $1E'$ and $3E'$ states. Because of the difference, a different χ_i contribution to bandwidth is expected for the third IT transition when compared to the first two.

From the analysis above, there should be three components to the IT band and the spacings between them should be related by eq 9 and 10 (see Figures 6 and 7 for the definitions of the various

$$\Delta E_1 = E_{1T,2} - E_{IT,1} = E_{SO,1} \quad (9)$$

$$\Delta E_2 = E_{IT,3} - E_{IT,1} = E_{SO,2} \quad (10)$$

energy quantities). For the osmium mixed-valence dimer, two of the expected three IT components are observed with an energy spacing between them of ca. 4800 cm^{-1}. From the $d\pi \rightarrow d\pi$ absorption bands for Os(III) the first transition occurs at $E_{SO,1} = 4000\ cm^{-1}$. Based on this value, it is straightforward to assign the band at 6000 cm^{-1} as the lowest energy IT band, IT,1. It should be noted that only the ground state of the initial Os(III) site, $1E'(i)$, where (i) is used to denote the initial Os(III) site before optical charge transfer, has an appreciable population at room temperature. Consequently, "hot band" transitions involving the higher states $2E'(i)$ and $3E'(i)$ are unimportant.[24] In terms of the initial states at Os(III) before charge transfer ($1E'(i)$, $2E'(i)$, $3E'(i)$) and the final states after charge transfer ($1E'(f)$, $2E'(f)$, and $3E'(f)$), the band at 6000 cm^{-1} assigned to $E_{IT,1}$ corresponds to the transition Os^{II}–$Os^{III}(1E'(i)) \rightarrow Os^{III}(1E'(f))$–$Os^{II}$.

It follows that the second IT band, which occurs at 10 800 cm^{-1}, can be assigned to the transition Os^{II}–$Os^{III}(1E'(i)) \rightarrow Os^{III}$-$(2E'(f))$–$Os^{II}$, since $2E'$ occurs ca. 4000 cm^{-1} above $1E'$. The energy difference between the two transitions, $\Delta E_1 \approx 4800\ cm^{-1}$, is in reasonable agreement with the energy of the first SO band, $E_{SO,1} = 4000\ cm^{-1}$, especially considering the assumptions required

(24) That the existence of electronic structure in the IT band region has its origin in electronic excitation from the site *initially* Os(II) is shown by comparisons with related Ru(II)–Os(III) dimers. For example, for the dimers $(bpy)_2ClRu^{II}(4,4'\text{-bpy})M^{III}Cl(bpy)_2^{3+}$ (M = Ru, Os), single, structureless IT bands are observed with roughly the same half-widths.[25]

(25) Goldsby, K. A.; Sullivan, B. P.; Meyer, T. J., manuscript in preparation.

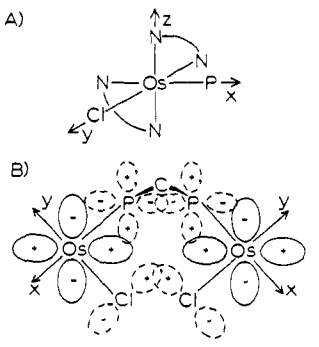

Figure 8. (A) Coordinate axes for the $(bpy)_2ClOs(PPh_2CH_2-)$ subunits. (B) Probable central geometry for the dimer $[(bpy)_2ClOs(PPh_2CH_2Ph_2P)OsCl(bpy)_2]^{3+}$. The Os d_{xy} orbitals are shown as the solid lines and the P d_{xy} and Cl p_x orbitals by the dashed lines. The diagram suggests that considerable overlap can be gained by mixing the metal and ligand orbitals.

in obtaining λ_{max} for the lowest energy IT band from the difference spectrum.

Upon assigning the two broad bands in the near-IR to the first and second IT transitions, the absence of a third band attributable to the transition, Os^{II}–$Os^{III}(1E'(i)) \rightarrow Os^{III}(3E'(f))$–$Os^{II}$, in the spectrum is easily accounted for. From eq 9 and 10, $E_{IT,3}$ would be expected to occur at $E_{IT,2} + (E_{SO,2} - E_{SO,1}) \approx 13\,300\ cm^{-1}$. At this high energy, the relatively weak IT band would be masked by intense charge-transfer bands (note Figure 2).

The intensity of the transition IT,2 ($1E'(i) \rightarrow 2E'(f)$) is observed to be 1.5 times as large as that for the transition IT,1 ($1E'(i) \rightarrow 1E'(f)$). The intensities of the three different IT transitions should be proportional to the amount of orbital overlap between the three different $d\pi$ orbitals on Os(II) with the $d\pi$ orbital containing the hole at Os(III) and therefore indicative of the mixing between the initial—$Os^{II}(A_1)$–$Os^{III}(1E')$—and final—$Os^{III}(1E')$–$Os^{II}(A_1)$, $Os^{III}(2E')$–$Os^{II}(A_1)$, and $Os^{III}(3E')$–$Os^{II}(A_1)$—IT states. Thus, the intensity differences between IT,2 and IT,1 must reflect differences in the orbital composition between $1E'$ and $2E'$. The extent of mixing between states can be easily reduced to a one electron overlap-type integral between the location of the "hole" in the initial state $1E'(i)$ and its location in the final state $1E'(f)$, $2E'(f)$, or $3E'(f)$. Since the orbital component characterizing $1E'(i)$ is constant for all three integrals, the problem of identifying the origins of the intensity differences reduces to establishing the orbital locations of the "hole" in the states $1E'(f)$, $2E'(f)$, and $3E'(f)$.

We will assume that one of the three orbitals d_{xy}, d_{yz}, and d_{xz} dominates in carrying the intensity of the transition in that the overlap of this orbital on Os(II) with the orbital on Os(III) containing the "hole" is much better than for the other two. Knowledge of the orbital composition of the holes in the three Os(III) SO states would allow the identity of the orbital which dominates the transition intensity to be established. Solution of the spin–orbit coupling matrix for $[(bpy)_2ClOs(PPh_3)]^{2+}$ (the monomeric analog of the dimer is a good model for the dimer since the $d\pi \rightarrow d\pi$ transitions occur at almost exactly the same energies as in the dimer) shows that only d_{xy} makes a greater contribution to the hole orbital in $2E'$ than to $1E'$.[20] Note Figure 8 for the definition of d_{xy}. Since the transition $1E'(i) \rightarrow 2E'(f)$ (IT,2) is more intense than $1E'(i) \rightarrow 1E'(f)$ (IT,1) by a factor of 1.5, it can be concluded that d_{xy} must be the dominant orbital. The intensities of the IT bands should depend on the d_{xy} character in the various SO states. By squaring the contributions of d_{xy} to each of the SO states, the predicted relative intensities for the three IT bands are 0.30, 0.58, and 0.11 in order of increasing energy for the transitions: IT, $1[1E'(i) \rightarrow 1E'(f)]$, IT,$2[1E'(i) \rightarrow 2E'(f)]$, IT,$3[1E'(i) \rightarrow 3E'(f)]$.[20]

That d_{xy} should be the critical orbital in terms of orbital overlap between Os(II) and Os(III) can also be determined from the probable geometry of the dimer. Using molecular models, it is found that the small bite angle of the bridging ligand forces the two Os subunits to a position of close contact. Because of the

greater size of the bpy groups, steric interactions are minimized by having the Cl groups at the face to face sites as shown in Figure 8. Such a structure results in having the Os, P, and Cl atoms lying essentially in a plane, with the methylene bridge of $PPh_2CH_2Ph_2P$ puckering out of the plane. The d_{xy} orbitals lie in the P,Os,Cl plane and are shown by the solid lines in Figure 8. The configuration shown results in good overlap between d_{xy} orbitals, which is no doubt enhanced by the mixing of d_{xy} with the P(d) and Cl(p) orbitals that lie in the plane, as shown in the figure.

With the assumption that the intensity of the IT bands is dependent upon the d_{xy} overlap, observed band intensities should be porportional to the square of the coefficient of the d_{xy} orbital in the $d\pi$ wave function of the "hole" for each state, as noted above. On this basis, it is expected that the transition $1E'(i) \rightarrow 2E'(f)$ should be ca. twice as intense as the transition $1E'(i) \rightarrow 1E'(f)$. The observed ratio is only a factor of 1.5. The discrepancy probably arises from two sources: (1) uncertainties in the assumptions used to obtain orbital compositions in the spin–orbit coupling treatment and (2) although d_{xy} is the most important source of IT band intensity, it is not the sole source.

An interesting and important result of the analysis given here is its application to the analogous Ru dimer where discrete IT transitions are not observed but rather a borad manifold with λ_{max} at 8020 cm^{-1} (see Figure 1). The experimental bandwidth for the Ru dimer exceeds that calculated by eq 5. An important contribution to the excess bandwidth is, no doubt, the presence of spectral components arising from the transitions involving the three SO states. The failure to resolve the three components for the Ru dimer at room temperature is an expected consequence of the smaller spin–orbit coupling constant for Ru compared to Os ($\lambda_{Ru} \approx {}^1/_3\lambda_{Os}$), which leads to a lesser splitting between the SO states. In addition, the smaller value for λ requires that the extent of mixing of the $d\pi$ orbitals will be less and consequently that the transition $Ru^{II}(A_1)$–$Ru^{III}(1E') \rightarrow Ru^{III}(2E')$–$Ru^{II}(A_1)$ will dominate the intensity of the IT manifold. In fact, the results of approximate calculations suggest that the relative intensity ratios are 0.23, 0.69, and 0.08 for the transitions to the 1E′, 2E′, and 3E′ states, respectively.[20] When taken together the two effects probably explain the absence of electronic structure for the Ru^{II}–Ru^{III} dimer.

Even though multiple IT transitions are not observable for the Ru dimer, the conclusion that they exist is extremely important and must be taken into account in any interpretation of IT spectral properties. The complexities introduced by multiple SO states extend to other complexes of Ru including those based on $(NH_3)_5Ru^{III}$ or $(NH_3)_5Ru^{II}$ groups and, for that matter, should be of nonnegligible importance for *all* second- and third-row transition metals where the spin–orbit coupling constant, λ, is appreciable in magnitude.

Returning to the Ru–bpy dimer, since it is expected that the IT manifold is dominated by the transition $1E'(i) \rightarrow 2E'(f)$, λ_{max} for the absorption manifold should provide a good estimate for $E_{IT,2}$. Calculations for the Ru dimer based on the model mentioned above show that the $1E'(i) \rightarrow 1E'(f)$ component of the IT manifold should occur at ca. 1700 cm^{-1} below the $1E'(i) \rightarrow 2E'(f)$ transition.[20] Thus, the predicted energy of $E_{IT,1}$ for the Ru dimer is ca. 6400 cm^{-1}, which is very close to $E_{IT,1}$ for the Os dimer at ca. 6000 cm^{-1}. That the energies of the two transitions should be nearly the same is not surprising. The structures at the Ru and Os sites should be essentially identical given the similar ionic radii for the two metals when in the same oxidation state, so that contribution from solvent vibrational trapping should be the same for both dimers. As noted above, that χ_0 is the same for both dimers is shown by the data in Figure 5 since the slopes of the lines are the same within experimental error. Furthermore, given the similarities in metal–ligand bond distances[26] and the fact that electronic structures at the Ru and Os sites are analogous, it may not be unreasonable to expect that χ_i could also be very similar for the two dimers.

Table II. Near-Infrared Spectral Data for the IT bands of $[(bpy)_2ClOs(PPh_2CH_2Ph_2P)OsCl(bpy)_2]^{3+}$ in CD_3CN

transition	$10^{-3}\cdot\lambda_{max}$, cm^{-1}	ϵ_{max}, M^{-1} cm^{-1}
$Os^{II}(A_1)$–$Os^{III}(1E') \rightarrow Os^{III}(1E')$–$Os^{II}(A_1)$	6.0	100
$Os^{II}(A_1)$–$Os^{III}(1E') \rightarrow Os^{III}(2E')$–$Os^{II}(A_1)$	10.8	140
$Os^{II}(A_1)$–$Os^{III}(1E') \rightarrow Os^{III}(3E')$–$Os^{II}(A_1)$	(13.3)[a]	

[a] Calculated from $E_{IT,3} = E_{IT,2} + (E_{SO,2} - E_{SO,1})$, which may be obtained by subtracting eq 9 from eq 10.

The Vibrational Barrier to Electron Transfer. Band properties and assignments for the near-IR bands of the Os(III) monomer and Os(II)–Os(III) and Os(III)–Os(III) dimers are summarized in Tables I and II. The dependence of the transition energy of IT,2 on solvent has been mentioned. In the limit of weak electronic coupling, the contribution of electronic delocalization to E_{IT} is negligible and the energy of an IT band depends on χ_i and χ_0 as shown in eq 11.[4,22] Including the solvent (medium) dependence

$$E_{IT} = \chi_i + \chi_0 \tag{11}$$

$$E_{IT} = E_{IT,1} = \chi_i(1E') + e^2\left(\frac{1}{a_1} - \frac{1}{d}\right)\left(\frac{1}{D_{op}} - \frac{1}{D_S}\right) \tag{12}$$

explicitly as in eq 7a gives eq 12. From eq 12, an extrapolation of $(1/D_{op} - 1/D_S)$ to the intercept should give an experimental estimate for χ_i.[1-5] However, it is clear that for the osmium mixed-valence dimer, eq 12 can only be applied to the lowest IT band. For the other two transitions, the absorption band energies include the energies of 2E′ and 3E′ above 1E′, as shown in eq 13 and 14.[4,22] As noted above, eq 13 and 14 rely on the assumption

$$E_{IT,2} = E_{SO,1} + \chi_i(2E') + e^2\left(\frac{1}{a_1} - \frac{1}{a}\right)\left(\frac{1}{D_{op}} - \frac{1}{D_S}\right) \tag{13}$$

$$E_{IT,3} = E_{SO,2} + \chi_i(3E') + e^2\left(\frac{1}{a_1} - \frac{1}{d}\right)\left(\frac{1}{D_{o+}} - \frac{1}{D_S}\right) \tag{14}$$

that χ_0 is independent of SO state, which is obviously a reasonable assumption given the $d\pi \rightarrow d\pi$ nature of the transition between SO states. From the extrapolation of the solvent dependence data for $E_{IT,2}$ in Figure 6 to $\chi_0 = 0$ and using $E_{SO,1} = 4000$ cm^{-1} from the near-IR spectrum gives $\chi_i(2E') = 4100$ cm^{-1} for the Os dimer. Recall from the previous discussion that $\chi_i(1E') \approx \chi_i(2E') \neq \chi_i(3E')$. The major contribution to χ_i is probably from vibrations ν(Os–Cl) in nature, a point that we are investigating experimentally, based on infrared and X-ray crystallographic studies.[27] It should be noted that the procedure described here for the estimation of χ_i is based on a classical approach which is, in fact, inappropriate since ν(Os–Cl) = 300–400 cm^{-1}. A more detailed analysis of the spectra will be given in a later manuscript.

For the Ru dimer it was concluded above that $E_{IT,1}(Ru) \approx E_{IT,1}(Os)$ and that $\chi_0(Ru) = \chi_0(Os)$. Consequently, it must follow that $\chi_i(Ru) \approx \chi_i(Os)$. In earlier work on related Ru dimers no attempt was made to account for the SO components in the IT manifold. Rather, band maxima for the IT absorption manifolds were used in plots of E_{op} vs. $(1/D_{op} - 1/D_s)$. As a consequence, the values reported in earlier work for χ_i are an overestimate by 1500–2000 cm^{-1}.

Electronic Delocalization. In the ground state of the dimer, $Os^{II}(A_1)$–$Os^{III}(1E')$, there are three contributions to electron delocalization. They arise from wave function overlap between the wave function containing the hole at Os(III), $d\pi_3$, and the three $d\pi$ wave functions at Os(II). The total extent of delocalization of the unpaired electron from Os(II) to Os(III) (α^2) is relatively small as might have been expected given the nature of the bridging ligand. Estimates for the extent of delocalization

(26) Griffith, W. P. "The Chemistry of the Rarer Platinum Metals", Interscience Publishers: New York, 1967; p 39.

(27) Eggleston, D. S.; Goldsby, K. A.; Hodgson, D. J.; Meyer, T. J., manuscript in preparation.

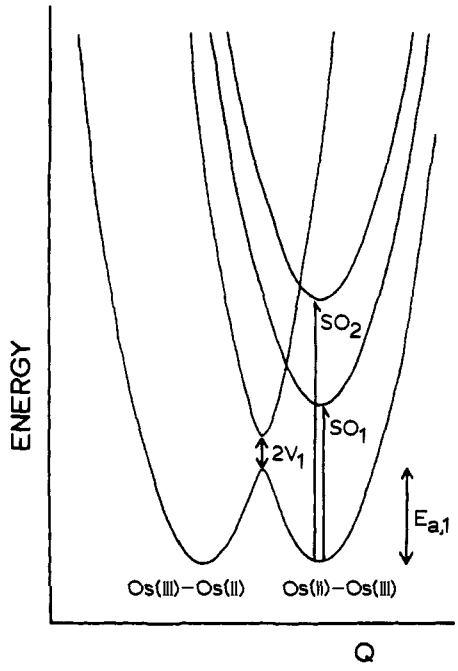

Figure 9. Energy-coordinate diagram for a trapping vibration including the effects of electronic delocalization for the dimer $[(bpy)_2ClOs(PPh_2CH_2Ph_2P)OsCl(bpy)_2]^{3+}$. Q is the coordinate for the trapping vibration.

can be made from IT band intensities. As shown by Hush, approximate values of α^2 can be calculated by using eq 15[4a] where

$$\alpha^2 = ((4.2 \times 10^{-4})\epsilon_{max}\Delta\bar{\nu}_{1/2})/(d^2E_{op}) \quad (15)$$

E_{op} and $\Delta\bar{\nu}_{1/2}$ are in inverse centimeters and d, the distance between redox sites, is in angstroms. For the Ru and Os dimers, the situation is complicated by the fact that there are three overlaps to account for involving the orbitals $d\pi_1$, $d\pi_2$, and $d\pi_3$ at the M(II) site and $d\pi_3$ at M(III). Consequently, there are three contributions to α^2: $\alpha^2 = \alpha_1^2 + \alpha_2^2 + \alpha_3^2$. Associated with electronic delocalization is a resonance energy, V,[28,29] which can be calculated from α and the energy of an IT band as shown in eq 16. For

$$V = \alpha E_{op} \quad (16)$$

the Ru(II)–Ru(III) dimer there is no direct evidence for resolved electronic structure. However, using the *total* absorption band gives $\alpha^2 = 1.3 \times 10^{-4}$ and $V = 92$ cm^{-1} in CD_3CN solution.[10] From the discussion above, α^2 and V are probably dominated by the transition 1E′(i) → 2E′(f). For the Os dimer, two of three IT bands are resolved (note Figure 4). Using the properties of the two bands gives $\alpha_1^2 \approx 8.7 \times 10^{-4}$ and $\alpha_2^2 = 6.7 \times 10^{-4}$. From the results of the spin–orbit coupling analysis mentioned in a previous section, the contribution to electronic delocalization from $d\pi_3$(Os(III))–$d\pi_3$(Os(II)) overlap which leads to the intensity for $E_{IT,3}$ is predicted to be relatively small. Summing the individual contributions for the Os dimer ($V_1 \approx 180$ cm^{-1}, $V_2 = 280$ cm^{-1}) gives $V \geq 460$ cm^{-1}. The enhanced electronic delocalization suggested for the Os dimer is worth noting. In an earlier study based on the ion pairs

$$M^{II}(CN)_6^{4-}, Ru^{III}(NH_3)_5(py)^{3+}$$

(M = Fe, Ru, Os) it was concluded that α^2 is approximately the same for M = Fe, Ru and only slightly larger for M = Os.[6b] The comparison between the two results might suggest that the greater delocalization for the Os dimer has its origin in greater Os–P mixing rather than greater through-space overlap.

Optical and Thermal Electron Transfer. In Figure 9 is shown an energy-coordinate diagram for a trapping vibration which illustrates the relationships between the IT and $d\pi \rightarrow d\pi$ (SO) transitions. The diagram is also of value in interrelating optical and thermal electron transfer. It includes the effects of electronic delocalization which causes a mixing of the IT states to give two new states. The effect of mixing is illustrated in Figure 9 for the two states involved in the lowest energy IT transition, $Os^{II}(A_1)$–$Os^{III}(1E')$ and $Os^{III}(1E')$–$Os^{II}(A_1)$. In the diagram the energy splitting between the two new states is $2V_1$ at the intersection region and the splitting between states is dependent both upon V and the coordinate of the trapping vibration.[1-5,22]

Because of the existence of multiple SO states at Os(III), there are three different channels for thermal electron transfer between Os(II) and Os(III) involving the ground state, $Os^{II}(A_1)$–$Os^{III}(1E')$. They are shown in eq 17. In the classical limit, thermal electron

$$Os^{II}(A_1)–Os^{III}(1E') \xrightarrow{k_{et,1}} Os^{III}(1E')–Os^{II}(A_1) \quad (17a)$$

$$Os^{II}(A_1)–Os^{III}(1E') \xrightarrow{k_{et,2}} Os^{III}(2E')–Os^{II}(A_1) \quad (17b)$$

$$Os^{II}(A_1)–Os^{III}(1E') \xrightarrow{k_{et,3}} Os^{III}(3E')–Os^{II}(A_1) \quad (17c)$$

transfer can only occur in the intersection region between the potential curves shown in Figure 9 because of the necessity of energy conservation during the transition. In this limit and assuming that electron transfer is slow on the vibrational timescale, the rate constant for electron transfer, k_{et}, is given by eq 18.[1b,30]

$$k_{et} = \nu_e \exp[-(E_a/RT)] \quad (18)$$

In the limit that V is negligible, E_a is given by eq 19.[4,22]

$$E_a = (\chi + \Delta E)^2/4\chi \quad (19)$$

It is worthwhile to consider the possible role played by the higher energy SO states in thermal electron transfer. For example, consider thermal electron transfer to give Os(III) in the first SO excited state, $k_{et,2}$, in eq 17b. Compared to the ground-state reaction, $k_{et,1}$ in eq 17a, the energy of activation is larger since $\Delta E = E_{SO,1}$ for $k_{et,2}$ and $\Delta E = 0$ for $k_{et,1}$. However, the resonance energy is greater for the excited state channel and since $V_2 > V_1$, the preexponential term for $k_{et,2}$ will be greater than the preexponential term for $k_{et,1}$. Using the values $V_1 \approx 180$ cm^{-1}, $V_2 = 280$ cm^{-1}, $\Delta E = E_{SO,1} = 4000$ cm^{-1}, and eq 18 and 19 give the prediction that thermal electron transfer should be dominated by the ground state channel since $k_{et,1} \approx 10^5 k_{et,2}$. Nonetheless, this may not be a general result. For dimers containing first- or second-row transition metals where λ is smaller, the splitting between the SO states will be less, as will be the mixing of the zero-order $d\pi$ orbitals. In a situation where ΔE is small and $V_2 \gg V_1$, SO excited states could provide significant and perhaps dominant channels for thermal electron transfer.

Acknowledgment is made to the Army Research Office (Durham) under Grant no. DAAG29-79-C-0044 for support of this research and to the Morehead Foundation of the University of North Carolina for a fellowship for E.M.K.

Registry No. *cis*-$[(bpy)_2OsCl_2]$, 79982-56-2; $[(bpy)_2ClOs(PPh_2CH_2Ph_2P)OsCl(bpy)_2](PF_6)_2$, 85370-07-6; $[(bpy)_2ClOs(PPh_2CH_2Ph_2P)OsCl(bpy)_2](PF_6)_4$, 85370-09-8; $[(bpy)_2ClOs(PPh_2CH_2Ph_2P)OsCl(bpy)_2](PF_6)_3$, 85370-11-2; $[(bpy)_2ClOs(PPh_3)]^{2+}$, 85370-12-3.

(28) Mulliken, R. S.; Person, W. B. "Molecular Complexes: A Lecture and Reprint Volume", Wiley-Interscience: New York, 1969; p 10.
(29) Mayoh, B.; Day, P. *J. Am. Chem. Soc.* **1972**, *94*, 2885.
(30) (a) Brunschwig, B. S.; Logan, J.; Newton, M. O.; Sutin, S. *J. Am. Chem. Soc.* **1980**, *102*, 5798. (b) Sutin, N. *Acc. Chem. Res.* **1982**, *15*, 275.